Solvent perturbations of extravalence excitations of atomic Xe by rare gases at high pressures

Itzhak Messing, Baruch Raz, and Joshua Jortner

Department of Chemistry, Tel-Aviv University, Tel-Aviv, Israel
(Received 20 May 1976)

In this paper we present the results of an experimental study of the lowest doublet excitations ($^1S_0 \rightarrow {}^3P_1$ and $^1S_0 \rightarrow {}^1P_1$) of atomic xenon in dense supercritical fluid neon and helium and the $^1S_0 \rightarrow {}^1P_1$ xenon excitation in dense supercritical and subcritical fluid argon. The spectral shift, the linewidth, the first moment, and the second moment of the absorption bands exhibit a strong density and a weak temperature dependence. The semiclassical statistical theory of line shapes was applied for the calculations of the first moment, the second moment, and the entire line shape. By fitting to the experimental moments over a broad density range, the excited state guest–host interaction potential parameters were derived. An analysis of the density dependence of the splitting and of the intensity ratio of the Xe doublet perturbed by high pressure rare gases was provided.

I. INTRODUCTION

Spectral perturbations of atomic excitations induced by foreign atoms at moderately low pressures were handled in terms of Margenau's statistical theory,[1] which accounts for spectral shifts[2] and for the appearance of satellite bands.[3] At higher densities the statistical theory has to be modified to account for correlation effects between the positions of the perturbing atoms. Recently Saxton and Deutch[4] and the present authors[5,6] have analyzed the (blue) spectral shifts and the line broadening in the absorption and emission[7] spectra of the lowest resonance line of atomic Xe, $Xe(^1S_0) - Xe(^3P_1)$[8] perturbed by supercritical and subcritical Ar. The statistical theory, extended to account for guest–host and host–host correlations, results in manageable expressions for the first moment and for the second moment of the absorption band which were expressed in terms of a difference guest–host interaction potential together with the solute–solvent and the solvent–solvent radial distribution functions. The theory was utilized to extract quite reliable information concerning the excited state $Xe(^3P_1) + Ar(^1S_0)$ pair potential. In this paper we present additional information regarding excited state potentials in rare-gas systems, extracted from the analysis of spectral perturbations. We report the results of an experimental study of solvent perturbations of the following transitions of atomic xenon: (1) $Xe(^1S_0) \rightarrow Xe(^1P_1)$ perturbed by Ar in the density range $\rho = 0.1-1.4$ g cm^{-3} ($1.5\times10^{-3}-2\times10^{-2}$ $\times10^{-2}$ atom Å^{-3}) in the temperature range 80–300 K. (2) $Xe(^1S_0) \rightarrow Xe(^3P_1)$ and $Xe(^1S_0) \rightarrow Xe(^1P_1)$ perturbed by Ne in the density range $\rho = 0.1-0.65$ g cm^{-3} ($3\times10^{-3}-1.9$ $\times10^{-2}$ atoms Å^{-3}) and in the temperature range 65–295 K. (3) $Xe(^1S_0) \rightarrow Xe(^3P_1)$ and $Xe(^1S_0) \rightarrow Xe(^1P_1)$ perturbed by He in the density range $\rho = 0.047 - 0.09$ g cm^{-3} ($7\times10^{-3}-1.35\times10^{-2}$ atoms Å^{-3}) and in the temperature range 113–295 K.

II. STATISTICAL THEORY OF LINE SHAPES

In this section we shall present a brief review of the statistical theory which will be subsequently applied for the analysis of our experimental data. The semiclassical approximation for the absorption lineshape function $\mathfrak{L}(\omega)$ for an allowed transition[9] is

$$\mathfrak{L}(\omega) = Z^{-1} \int \cdots \int \exp[-\beta W_g(\mathbf{R}_1 \cdots \mathbf{R}_N)]\, \delta[W_g(\mathbf{R}_1 \cdots \mathbf{R}_N) - W_e(\mathbf{R}_1 \cdots \mathbf{R}_N) + \hbar\omega - \hbar\omega_0] \prod_i d^3R_i , \quad \text{(II.1)}$$

$$Z = \int \cdots \int \exp[-\beta W_g(\mathbf{R}_1 \cdots \mathbf{R}_N)] \prod_i d^3R_i ,$$

where $W_g(\mathbf{R}_1, \mathbf{R}_2, \cdots \mathbf{R}_N)$ and $W_e(\mathbf{R}_1, \mathbf{R}_2 \cdots \mathbf{R}_N)$ denote the multidimensional adiabatic potential surfaces of the system in the ground and in the electronically excited state, respectively. $\mathbf{R}_1, \mathbf{R}_2 \cdots \mathbf{R}_N$ denote the position vectors of the host atoms relative to the guest atom. $\beta = (k_B T)^{-1}$, $\hbar\omega$ is the photon energy while $\hbar\omega_0$ corresponds to the guest atomic excitation at $\rho = 0$. Next, one has to invoke the additivity assumption for the potential surfaces which are thus approximated as superpositions of pair potentials

$$W_g(\mathbf{R}_1 \cdots \mathbf{R}_N) = \sum_i V_g(\mathbf{R}_i) + \sum_{i<m} U_g(|\mathbf{R}_i - \mathbf{R}_m|),$$
$$W_e(R_1 \cdots R_N) = \sum_i V_e(\mathbf{R}_i) + \sum_{i<m} U_g(|\mathbf{R}_i - \mathbf{R}_m|) . \quad \text{(II.2)}$$

$V_g(\mathbf{R}_i)$ and $V_e(\mathbf{R}_i)$ are the guest–host pair potentials in the ground and in the excited state of the Xe atom, respectively, while $U_g(|\mathbf{R}_i - \mathbf{R}_m|)$ corresponds to the host–host pair potential in the ground state. The difference guest–host pair potential is defined as

$$\Delta V(\mathbf{R}_i) = V_e(\mathbf{R}_i) - V_g(\mathbf{R}_i) . \quad \text{(II.3)}$$

From Eqs. (II.1)–(II.3) the line shape is recast in terms of a Fourier transform

$$\mathfrak{L}(\omega) = \frac{1}{2\pi} \int_{-\infty}^{\infty} dt \exp[it(\omega - \omega_0)]\, f(t) \quad \text{(II.4)}$$

where the generating function is

$$f(t) = \int \cdots \int P(\mathbf{R}_1, \mathbf{R}_2, \cdots \mathbf{R}_N) \exp\left[-i \sum_i \Delta V(\mathbf{R}_i) t\right] \prod_i d^3R_i . \quad \text{(II.5)}$$

$P(\mathbf{R}_1 \cdots \mathbf{R}_N)$ is the probability that one perturbating atom is at $\mathbf{R}_1$, a second atom at $\mathbf{R}_2$, etc.,

$$P(\mathbf{R}_1, \mathbf{R}_2, \cdots \mathbf{R}_N) = \exp[-\beta W_g(\mathbf{R}_1, \mathbf{R}_2 \cdots \mathbf{R}_N)]/Z . \quad \text{(II.6)}$$

The generating function can be expressed in terms of an exponential density expansion[3]

$$f(t) = \exp[A_1(t) + A_2(t) + \cdots] , \tag{II.7}$$

where the first term is

$$A_1(t) = 4\pi\rho \int_0^\infty dR R^2 g_{12}(R) \{\exp[-it\Delta V(R)] - 1\} , \tag{II.8a}$$

while the second term can be estimated using Kirkwood's superposition approximation[10]

$$A_2(t) = 4\pi\rho^2 \int_0^\infty dR_1 R_1^2 g_{12}(R_1) \{\exp[-it\Delta V(R_1)] - 1\} \times \int_0^\infty dR_2 R_2^2 g_{12}(R_2) \{\exp[-it\Delta V(R_2)] - 1\} (1/R_1R_2) \times \int_{|R_1-R_2|}^{|R_1+R_2|} S[g_{11}(S) - 1] dS , \tag{II.8b}$$

$g_{12}(R)$ is the solute–solvent radial distribution function (RDF), and $g_{11}(R)$ is the solvent–solvent RDF.

We now turn to a moment analysis of the line shape function. The Ith moment of $\mathfrak{L}(\omega)$, Eq. (II.4), is given by[11]

$$m_I = (i)^I \frac{d^I f(t)}{dt^I}\bigg|_{t=0} . \tag{II.9}$$

Equations (II.5) and (II.7) now result in

$$m_I = (i)^I \int \cdots \int \prod_i d^3R_i \left[-\sum_i i\Delta V(\mathbf{R}_i)\right]^I P(\mathbf{R}_1 \cdots \mathbf{R}_N) . \tag{II.10}$$

The lowest moments are now obtained in the form

$$m_0 = 1 ,$$

$$m_1 = N \int d^3\mathbf{R}_1 \Delta V(\mathbf{R}_1) P^{(1)}(\mathbf{R}_1) , \tag{II.11}$$

$$m_2 = N \int d^3\mathbf{R}_1 [\Delta V(\mathbf{R}_1)]^2 P^{(1)}(\mathbf{R}_1) + N(N-1) \int\int d^3\mathbf{R}_1 d^3\mathbf{R}_2 \Delta V(\mathbf{R}_1)\Delta V(\mathbf{R}_2) P^{(2)}(\mathbf{R}_1, \mathbf{R}_2) ,$$

where

$$P^{(i)}(\mathbf{R}_1 \cdots \mathbf{R}_i) = \int \cdots \int \prod_{i=i+1}^{N} d^3\mathbf{R}_i P(\mathbf{R}_1 \cdots \mathbf{R}_N) , \tag{II.12}$$

corresponds to the i-particles distribution function. The one-particle distribution function $P^{(1)}(\mathbf{R}_1)$ is

$$P^{(1)}(\mathbf{R}_1) = (\rho/N) g_{12}(R_1) , \tag{II.13a}$$

while the two-particles distribution function can be expressed using the Kirkwood superposition approximation[12]

$$P^{(2)}(\mathbf{R}_1, \mathbf{R}_2) = \frac{(N-2)!}{N!} \rho^2 g_{12}(R_1) g_{12}(R_2) \times g_{11}(|\mathbf{R}_1 - \mathbf{R}_2|) . \tag{II.13b}$$

Eqs. (II.11) and (II.13) yield the following results for the moments of the spectral distribution

$$m_1 = 4\pi\rho \int_0^\infty dR R^2 \Delta V(R) g_{12}(R) , \tag{II.14a}$$

and

$$m_2 = m_1^2 + 4\pi\rho \int_0^\infty dR R^2 [\Delta V(R)]^2 g_{12}(R) + 8\pi^2\rho^2 \int_0^\infty \int_0^\infty dR_1 dR_2 R_1^2 R_2^2 \Delta V(R_1) \times \Delta V(R_2) g_{12}(R_1) g_{12}(R_2) \times (1/R_1R_2) \int_{|R_1-R_2|}^{|R_1+R_2|} dS S[g_{11}(S) - 1] . \tag{II.14b}$$

The experimental first moment $M_1 = m_1$ and the spectral dispersion $M_2 = (m_2 - m_1^2)^{1/2}$ can be analysed in terms of Eq. (II.14). It is important to emphasize at this stage that the first and the second quantum mechanical moments of a strongly allowed transition are correctly given by the semiclassical approximation.[13] The only approximations inherent in Eq. (II.14) are the pairwise approximation, Eq. (II.2) for the potential surfaces and the Kirkwood superposition approximation, Eq. (II.13b), for the three-body correlation effects.

III. EXPERIMENTAL PROCEDURE

The absorption spectra of Xe/Ar; Xe/Ne and Xe/He mixtures were monitored in the spectral region 1150–1600 Å. The experimental setup was the same one used previously,[6] except that single beam detection was applied. A conventional Tanaka light source[14] (Ar and Kr lamps) was used. We have employed a McPherson 225 vacuum spectrograph equipped with a grating of 1200 lines/mm. The resolution for 150 μm slit width was 1.5 Å (90 cm^{-1} at 1300 Å). Transmitted light was detected by an EMI 9514S photomultiplier coated with Sodium Salicylate converter. The signal was amplified before being chart recorded. The high pressure absorption cell and the gas handling system were described elsewhere.[6] In experiments with Ne and He the cell was cooled by the flow of cold He from a liquid He container and therefore was supplied with a radiation shield. The temperature was monitored with an accuracy of ± 2 K by a chromel/Fe : Au thermocouple. In experiments where solvent perturbation by He and Ne were studied the procedure was as follows. The mixtures were prepared by first introducing Xe at pressures 0.05–0.10 torr from the gas handling system into the cell. Subsequently, Ne or He (Matheson Research Grade) were introduced directly from the original cylinder into the cell. The amount of gas in the cell was measured at the end of each experiment by expanding into the gas handling system. The highest pressure applied was 400 atm at 300 K and the temperature range covered was 300–24 K. The general procedure of determining the density inside the cooled optical cell was already described.[6] The pressures at the two different parts of the cell, which are characterized by different temperatures, were expressed as functions of density using the appropriate expressions for the equation of state at room temperature[15] and at the cooled part.[16] The densities which cause an equilization of pressures were evaluated by the Newton–Raphson root finding method. The upper limit for the fluid density in Xe/Ne and Xe/He systems was determined by the solubility limit of Xe in these fluids. In experiments with Ar, the apparatus, sample preparation and density determination method are the same as described in Ref. 6.

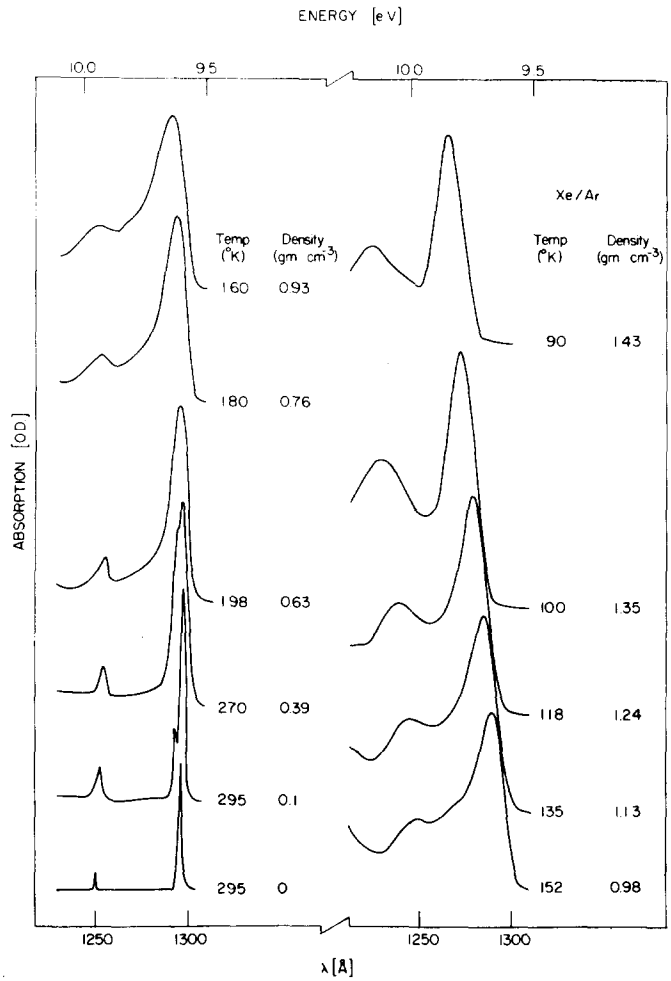

FIG. 1. Absorption spectra of Xe perturbed Ar in the wavelength range 1230–1300 Å.

IV. SOLVENT PERTURBATION OF Xe($^3P_1$) AND Xe($^1P_1$) BY Ar, Ne, AND He

In Fig. 1 we present the absorption spectra of Xe/Ar mixture ([Xe]/[Ar] = 10^{-6}) in the energy range 1230–1300 Å (9.5–10.1 eV) in the density region $\rho = 0.1 - 1.4$ g cm^{-3} (1.5×10^{-3}–2×10^{-2} atom Å^{-3}) and in the temperature range 80–300 K, spanning the effects of solvent perturbations from low pressure supercritical gas, throughout the dense supercritical and subcritical fluid. Two transitions are exhibited at low densities, the atomic transition to the Xe $6s'[\frac{1}{2}]$ state, i.e., $^1S_0 \rightarrow {}^1P_1$ (appearing at 1296 Å (9.59 eV) at $\rho \rightarrow 0$) and the atomic transition to the Xe $5d[\frac{1}{2}]$ state (appearing at 1250 Å (9.94 eV) for $\rho \rightarrow 0$). In what follows we shall consider solvent shifts of the former transition. At moderately low Ar densities $\rho \lesssim 0.3$ g cm^{-3} a single blue satellite band appears on the high energy side of the second [Xe($^1P_1$)] resonance line, in accord with previous observations.[17] At higher density, $\rho = 0.4$ g cm^{-3}, the satellite band considerably overlaps the broadened resonance line and for higher densities, $\rho > 0.4$ g cm^{-3}, the absorption spectrum merges into a single broadened absorption band which is blue shifted and further broadened with increasing Ar density. The features of solvent perturbations are specified in terms of the spectral shift Δ (relative to the atomic transition $\hbar\omega_0 = 77185$ cm^{-1}), the linewidth at half maximum δ, the first moment M_1, and the spectral dispersion M_2. The two latter observables can be confronted with the statistical theory discussed in Sec. II. Unfortunately, the intensity of the absorption band around ~ 10 eV increases appreciably with increasing density and in the density region $\rho > 0.65$ g cm^{-3} the absorption in the range 1200–1270 Å (9.8–10.3 eV) overlaps the perturbed Xe($^1P_1$) band. This interesting effect, which will be discussed elsewhere,[18] prevents us from deriving reliable experimental data for M_1 and for M_2 in the density range $\rho > 0.65$ g cm^{-3}. The density and the temperature dependence of the spectral shift Δ are portrayed in Fig. 2. We find that Δ is temperature independent (within experimental accuracy limits of ± 60 cm^{-1}) throughout the entire temperature region $T = 80$–300 K. At low ($\rho < 0.3$ g cm^{-3}) densities the resonance line exhibits a red spectral shift while in the density region 0.3–1.4 g cm^{-3} a blue shift is revealed which shows a superlinear increase with increasing ρ. The density dependence of the linewidth at half maximum δ is presented in Fig. 3. In the density range $\rho > 0.7$ g cm^{-3} the contribution of the overlap of the high energy band was subtracted assuming that the perturbed Xe($^1P_1$) absorption band is symmetric. This inevitable procedure introduces some arbitrariness (accuracy of $\pm$ 10%) in the determination of δ. We note that δ increases almost linearly with increasing ρ up to $\rho \cong 1.0$ g cm^{-3} and reveals a weak density dependence in the high density range $\rho = 1.0$–1.4 g cm^{-3}. The temperature dependence of δ throughout the range 80–300 K is weak, within the experimental uncertainty claimed by us ($\pm$ 10%). The gross features of the density dependence of Δ and δ for the Xe($^1S_0$) $\rightarrow$ Xe($^1P_1$) transition perturbed by Ar are similar to those previously reported by us[6] for the Xe($^1S_0$) $\rightarrow$ Xe($^3P_1$) transition in fluid Ar.

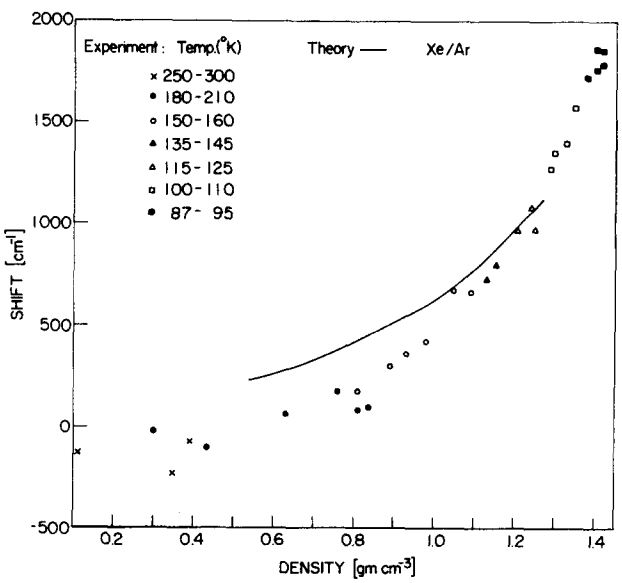

FIG. 2. Density dependence (in the temperature range 85–300 K) of the spectral shift at the maximum of the Xe $^1S_0 \rightarrow {}^1P_1$ absorption line perturbed by Ar relative to the atomic value $\hbar\omega_0 = 77185$ cm^{-1}. Experimental data are designated by points. The solid curve is the calculated first moment using best fit of excited state potential at high ($\rho \geq 0.1$ g cm^{-3}) densities.

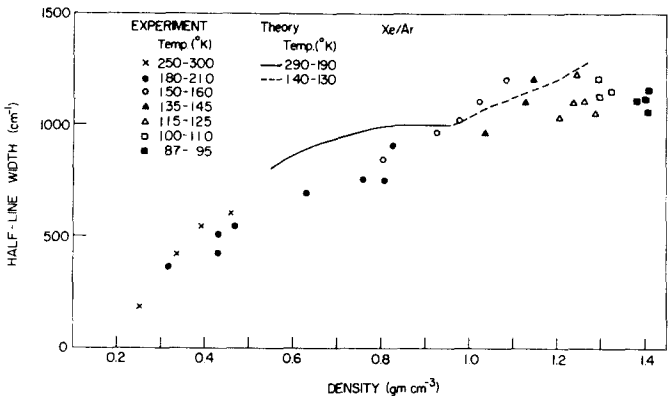

FIG. 3. Density dependence (in the temperature range 85–300K) of the linewidth at half maximum of the $Xe\,{}^1S_0 \rightarrow {}^1P_1$ transition perturbed by Ar. Experimental data are designated by points. The values at densities higher than 0.6 g cm^{-3} were obtained by assuming a symmetrical line shape. The curves represent the value of 2.4 M_2 calculated using best fit potential at high (>1.0 g cm^{-3}) densities.

In Figs. 4 and 5 we present the absorption spectra of Xe in the range 1500–1150 Å (8.4–10.3 eV) perturbed by Ne and by He. The perturbers densities were 0.1–0.65 g cm^{-3} (3×10^{-3}–1.9×10^{-2} atom Å^{-3}) for Ne over the temperature range 65–295 K and densities of 0.047–0.09 g cm^{-3} (7×10^{-3}–1.35×10^{-2} atom Å^{-3}) for He over the temperature range 113–295 K. We shall briefly discuss solvent perturbations of the $Xe(^1S_0) \rightarrow Xe(^3P_1)$ transition at 1470 Å (8.44 eV) and the $Xe(^1S_0) \rightarrow Xe(^1P_1)$ transition at 1296 Å (9.57 eV). We note that the two blue satellites[16] appearing at the high energy side of the first $Xe(^3P_1)$ line and the single blue satellite[17] on the high energy side of the $Xe(^1P_1)$ line at low pressure ($p \sim 100$–1000 torr) of these perturbing gases are smeared out at the lowest Ne density ($\rho = 3\times10^{-3}$ atom Å^{-3}, 0.1 g cm^{-3}) and at the lowest He density ($\rho = 7\times10^{-3}$ atom Å^{-3}, 0.047 g cm^{-3}) studied herein. The experimental data for M_1 and M_2 derived from these absorption spectra are summarized in Table I. The $Xe(^3P_1)$ transition is well separated from the higher bands and no problems are involved in the evaluation of the moments. The $Xe(^1P_1)$ state perturbed by Ne and by He weakly overlaps the Xe $5d[\frac{1}{2}]$ state located at ~10 eV, (1250 Å). As is evident from Figs. 4 and 5, this latter band is weak and its intensity is weakly dependent on the foreign gas density in contrast to the behavior of the Xe/Ar system where a strong density dependent absorption is exhibited in this density range. Thus in the Xe/Ne and Xe/He systems reliable experimental data for M_1 and for M_2 could be obtained.

V. EXCITED-STATE POTENTIALS

In order to calculate the first moment and the dispersion of the absorption line shapes it is necessary to know the difference potential ΔV, the guest–host RDF, $g_{12}(R)$, and the RDF $g_{11}(R)$ for the pure solvent. The ground state potential was taken in the Lennard-Jones form with well known[19] parameters which are reproduced in Table II. For the excited state solute–solvent pair potential we have chosen the exponential-6 three-parameter potential of the form

$$V(r) = \frac{\epsilon}{1-6/\alpha}\{(6/\alpha)\exp[\alpha(1-r/r_e)] - (r_e/r)^6\}, \quad (V.1)$$

where ϵ is the potential well depth, r_e the equilibrium distance, and α the steepness parameter. $g_{11}(R)$ for the Xe/Ar and for the Xe/Ne systems was calculated in two ways. First, using the simple Percus–Yevick hard-spheres model[20] (PYHS) at the reduced density $\rho^* = \rho\sigma_{11}^3$ and, second, by using the more accurate Percus–Yevick approximation for a Lennard-Jones fluid (PYLJ)[21] at the reduced density ρ^* and at the reduced temperature $T^* = k_BT/\epsilon_{11}$, where $\sigma_{11} = 3.36$ Å and $\epsilon_{11} = 1.2\times10^{-2}$ eV[19a] correspond to the Lennard-Jones potential parameters for the $Ar(^1S_0)$–$Ar(^1S_0)$ interaction. As we have shown elsewhere,[6] the theoretical results for M_1 and for M_2 are sensitive to the form of the solvent–solute RDF but rather insensitive to the fine details of the solvent–solvent RDF. Indeed, the values of M_2 calculated using the PYHS and PYLJ forms for $g_{11}(R)$ differ by less than 5% and consequently we preferred to use the simpler and more convenient PYHS approximation for $g_{11}(R)$. The RDF $g_{12}(R)$ for Xe/Ar and for Xe/Ne mixtures was calculated by applying the PYLJ approximation for a pure fluid with the Xe–Ar or with the Xe–Ne LJ potential parameters and by scaling for the binary mixtures using the procedure proposed by Deutch and Saxton.[4] Finally, for the Xe/He system, where the Saxton–Deutch scaling procedure for $g_{12}(R)$ is expected to be unreliable in view of the large size and the large mass difference between the two constituents, we have utilized the PYHS approximation both for the pure fluid[20] and for the mixture.[22]

To obtain theoretical information regarding the per-

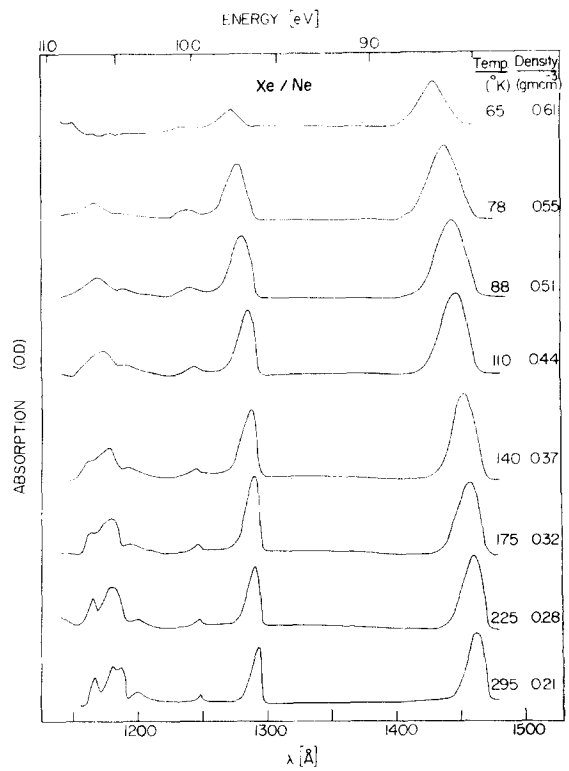

FIG. 4. Absorption spectra of Xe perturbed by Ne at the wavelength range 1150–1500 Å.

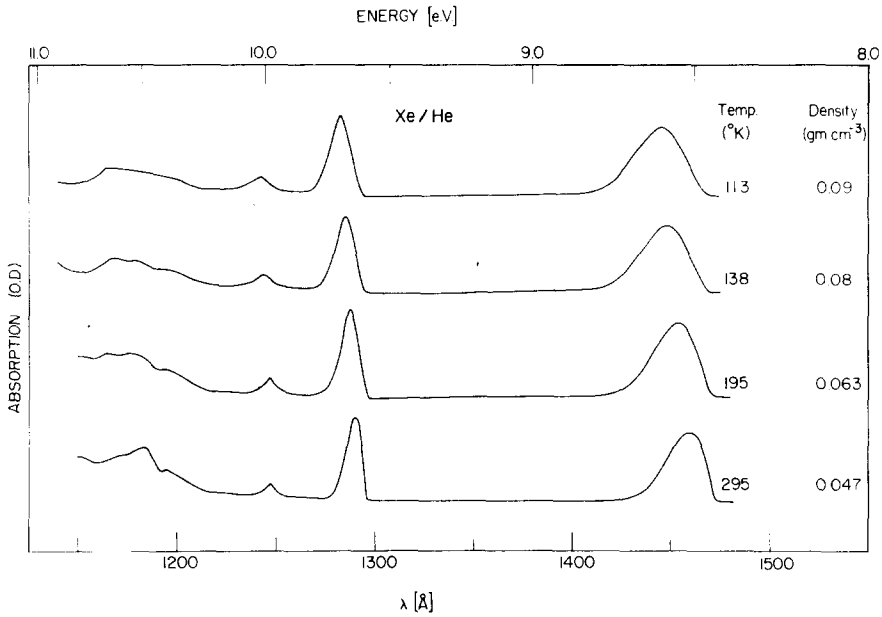

FIG. 5. Absorption spectra of Xe perturbed by He at the wavelength range 1150–1500 Å.

turbation of the $Xe(^1P_1)$ state by Ar we have assumed, in accordance with previous results[6] for the $Xe(^3P_1)$ state, that in the density range $\rho > 0.8$ g cm^{-3} the absorption band corresponding to this state is symmetrical, whereupon $\Delta \simeq M_1$. Furthermore, we assume that in this density range the second moment of the line shape is close to that corresponding to a Gaussian (as is the case for the $Xe(^3P_1)$/Ar system[6]) and we accordingly set $M_2 = 0.42\delta$. At lower ($\rho \sim 0.6$ g cm^{-3}) densities where the absorption band is asymmetric a direct evaluation of M_1 and M_2 from the experimental spectra was carried out. The best excited state potential parameters for this system are summarized in Table II, and are utilized in Table I and in Figs. 2 and 3 for the calculation of the density dependence of M_1 and of M_2. In the high density range the theoretical values of M_1 and of 2.38 M_2 fit quite well the experimental data Δ and for δ, respectively.

The analysis of the solvent perturbations of the $Xe(^3P_1)$

TABLE I. Density dependence of the first moment and of the dispersion of the resonance lines of Xe perturbed by high pressure rare gases.

Perturber Atom	Density g cm^{-3}	Density (atoms Å^{-3} $\times 10^{-3}$)	Temp. (°K)	M_1(exp) (cm^{-1})	M_2(exp) (cm^{-1})	M_1(calc) (cm^{-1})	M_2(calc) (cm^{-1})	Excited state potential ϵ (10^{-4} eV)	r_e (Å)	α
				$(^3P_1)$ Xe line $\{6s[\frac{3}{2}]$ 1470 Å$\}$						
Ne	0.21	6.5	295	465	310	545	360	2.5	5.9	15
Ne	0.31	9.2	175	755	385	725	400			
Ne	0.41	12.2	150	980	415	920	445			
Ne	0.51	15.2	78	1380	530	1200	460			
Ne	0.65	19.0	70	2000	540	1600	510			
He	0.09	13.5	113	1320	560	1210	580	1.5	6.35	15
He	0.08	12.0	138	1200	530	1050	550			
				$(^1P_1)$ Xe line $\{6s'[\frac{1}{2}]$ 1296 Å$\}$						
								120	4.5	15
Ar	0.63	9.5	200	320	500	300	380			
Ar	1.27	19.1	140	1150[a]	480[a]	1120	520			
								2.5	5.4	17
Ne	0.21	6.5	295	370	230	410	275			
Ne	0.31	9.2	175	530	310	550	300			
Ne	0.41	12.2	150	725	355	695	320			
Ne	0.51	15.2	78	1110	450	900	340			
Ne	0.65	19.0	70	1550	460	1180	370			
								1.5	6.0	15
He	0.09	13.5	113	870	340	770	360			
He	0.08	12.0	138	740	300	670	340			

[a]Comparison is made by assuming $M_1 = \Delta$(Shift) and $M_2 = 0.42\delta$ (half-line width).

TABLE II. Ground-state and excited-state potential parameters.

Perturber Atom	Xe Level	Potential Parameters: Excited-state (exp-6) ϵ (eV)	r_e(Å)	α	Ground-state (LJ) ϵ_{12}(eV)	σ_{12}(Å)	Reference
Ar	$5p'[\frac{3}{2}]_1$				1.6×10^{-2}	3.64	(1)
Ar	$6s[\frac{3}{2}]_1$	8×10^{-3}	4.6	15			(2)
Ar	$6s'[\frac{1}{2}]_1$	1.2×10^{-2}	4.5	15			(3)
Ne	$5p'[\frac{3}{2}]_1$				6.5×10^{-3}	3.5	(1)
Ne	$6s[\frac{3}{2}]_1$	2.5×10^{-1}	5.9	15			(3)
Ne	$6s'[\frac{1}{2}]_1$	2.5×10^{-1}	5.4	17			(3)
He	$5p'[\frac{3}{2}]_1$				4.3×10^{-3}	3.36	(1)
He	$6s[\frac{3}{2}]_1$	1.5×10^{-1}	6.4	15			(3)
He	$6s'[\frac{1}{2}]_1$	1.5×10^{-1}	6.0	15			(3)

[1]Reference 19. [2]Reference 6. [3]Present work.

and $Xe(^1P_1)$ excited states by Ne and He is conducted in Table I where the "best" excited state potential parameters to fit M_1 and M_2 throughout the entire density range are summarized in Table II. The agreement between the simple theory and experiment is within 20%. The uncertainty in the fit of the excited state potential parameters is $\Delta\epsilon = \pm 2\times10^{-3}$ eV (Ar), $\pm 1\times10^{-4}$ eV (Ne, He); $\Delta r_e = \pm 0.05$ Å (Ar), $\Delta r_e = \pm 0.3$ Å (Ne, He); $\Delta\alpha = \pm 1$.

From these data, together with the results of our previous work,[6] we have derived a set of quite reliable potential parameters (Table II) for the excited state potentials in some rare-gas systems. From these data three interesting conclusions emerge. First, the excited state potential of $Xe(^3P_1) + Y(^1S_0)$ where Y ≡ Ar, Ne, and He, is more repulsive than the corresponding $Xe(^1P_1) + Y(^1S_0)$ potential, that is the latter potential being characterized by a lower value of r_e. Second, the depth ϵ of the excited state potential for both $Xe(^3P_1) + Y(^1S_0)$ and $Xe(^1P_1) + Y(^1S_0)$ decreases from Y ≡ Ar to Y ≡ He, as expected. Third, we note that the equilibrium value r_e decreases in the order $r_e(\text{Ar}) < r_e(\text{Ne}) < r_e(\text{He})$. This is an unexpected result for the excited state potential as in the ground state σ_{12} and the equilibrium separation vary in the reverse order.

In Figs. 6(a)–(c) we present the excited state pair potentials obtained by us, together with the appropriate difference potentials. It is important to note that in all cases $\Delta V(R)$ is a smooth monotonically decreasing function of R. This observation raises an interesting problem concerning the appearance of the blue satellites on the high energy side of both the $Xe(^3P_1)$ and $Xe(^1P_1)$ transitions perturbed by Ar, Ne, and He at low densities. The semiclassical approximation attributes blue and red satellites to maxima and minima in $\Delta V(R)$, respectively.[3,23] In the case of $Xe(^3P_1) + Y(^1S_0)$ and $Xe(^1P_1) + (^1S_0)$ the appearance of two blue satellites in the former case and one blue satellite in the latter case would then infer a maximum in the difference potential, which is not the case. A more profound study of these satellite bands will be of interest.

The present treatment provides quite reliable theoretical estimates of the first moment and of the second moment of the absorption bands. A calculation of the entire energy dependent lineshape requires, in prin-

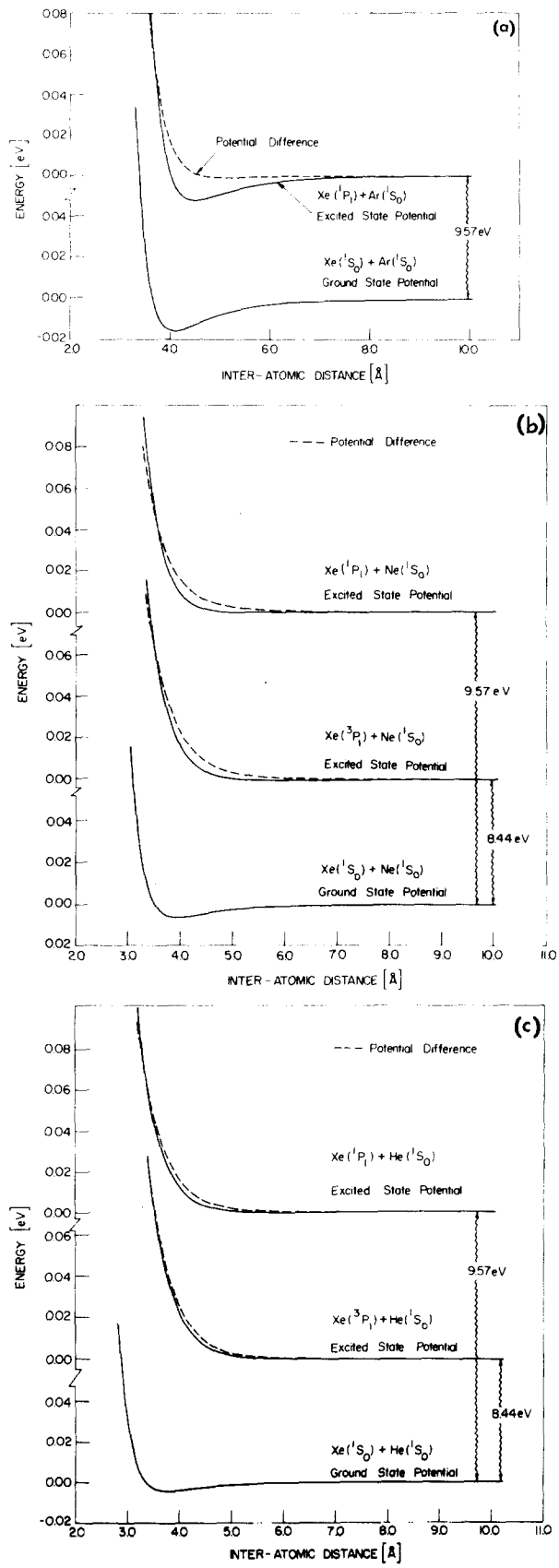

FIG. 6. Potential curves for the $Xe(^1S_0) + Y(^1S_0)$ potential and $Xe(^3P_1;\ ^1P_1) + Y(^1S_0)$ excited state potentials (solid curves) Y = Ar, Ne, He together with the difference potentials $\Delta V(r)$ (dashed curve). The potential parameters are given in Table II. (a) $Xe(^1S_0 \rightarrow {}^1P_1) + Ar(^1S_0)$ interaction potentials. (b) $Xe(^1S_0 \rightarrow {}^3P_1;\ ^1P_1) + Ne(^1S_0)$ interaction potentials. (c) $Xe(^1S_0 \rightarrow {}^3P_1;\ ^1P_1) + He(^1S_0)$ interaction potentials.

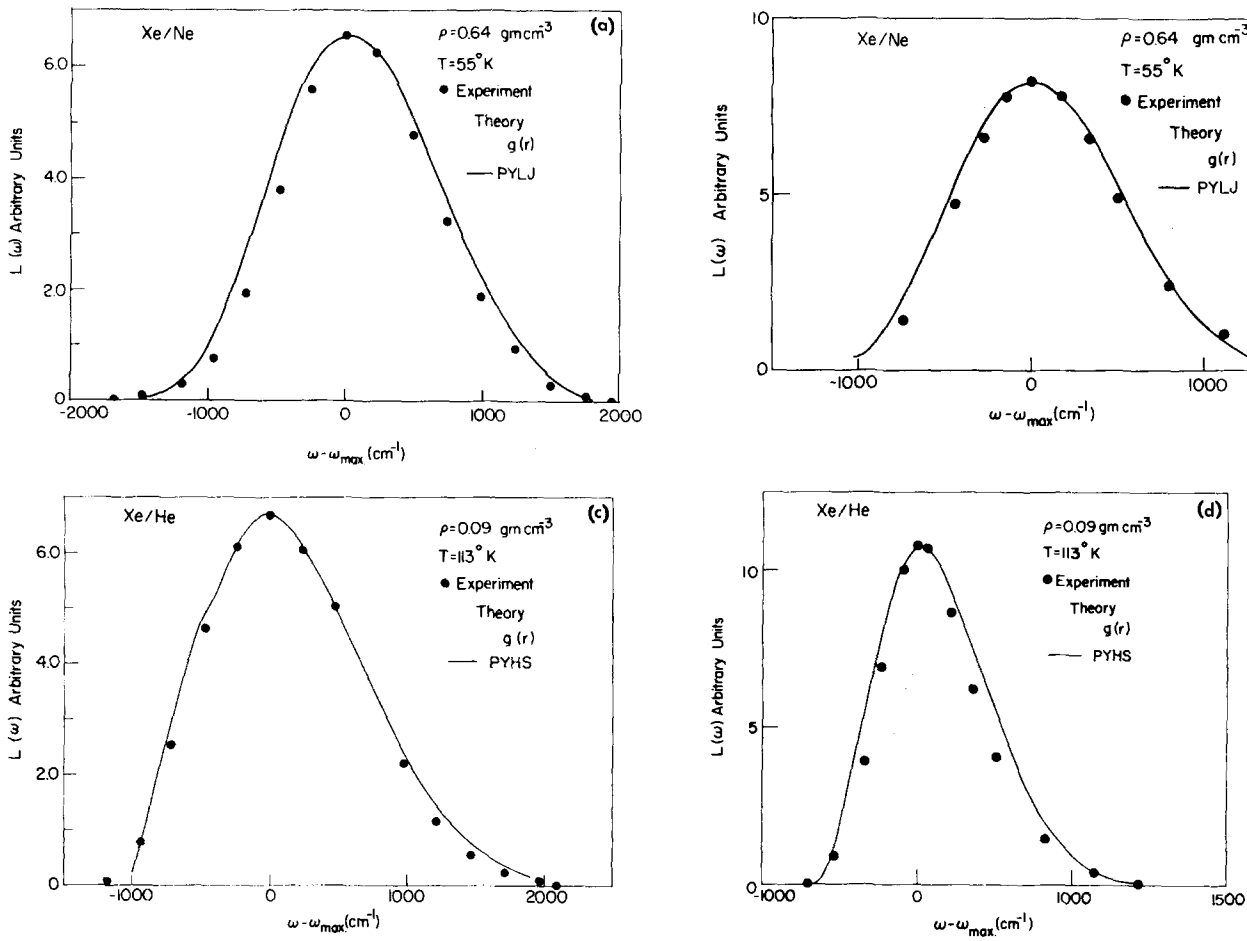

FIG. 7. Calculated line shapes (solid curves) for Xe/Ne and Xe/He incorporating two-body and three-body correlation effects. $f(t)=\exp[A_1(t)+A_2(t)]$ where $A_1(t)$ and $A_2(t)$ are given by Eqs. (II. 8a) and (II. 8b). The points represent experimental data. (a) Line shape for the Xe $^1S_0 \rightarrow {}^3P_1$ transition perturbed by Ne relative to band maximum $\hbar\omega_{max}=70050$ cm^{-1} (experiment) $\hbar\omega_{max}=69650$ cm^{-1} (calculated). PYLJ RDF for $g_{12}(R)$ was employed. (b) Line shape for the Xe $^1S_0 \rightarrow {}^1P_1$ transition perturbed by Ne relative to band maximum $\hbar\omega_{max}=78750$ cm^{-1} (experiment); $\hbar\omega_{max}=77650$ (calculation). PYLJ RDF for $g_{12}(R)$ was employed. (c) Line shape for the Xe $^1S_0 \rightarrow {}^3P_1$ transition perturbed by He relative to the band maximum $\hbar\omega_{max}=69370$ cm^{-1} (experiment); $\hbar\omega_{max}=69260$ cm^{-1} (calculation). PYHS RDF for $g_{12}(R)$ was employed. (d) Line shape for the Xe $^1S_0 \rightarrow {}^1P_1$ transition perturbed by He relative to the band maximum $\hbar\omega_{max}=78050$ cm^{-1} (experiment); $\hbar\omega_{max}=77950$ cm^{-1} (calculation). PYHS RDF for $g_{12}(R)$ was employed.

ciple, not only the low order $A_1(t)$ and $A_2(t)$ terms in Eq. (II.7) but also higher order terms. It is of some interest to evaluate the entire line shape, incorporating the effects of the two-body and three-body correlation effects and disregarding the effects of higher solvent–solvent correlations. Accordingly, we have performed a calculation of the line shape, Eq. (II.4), using the generating function $f(t)=\exp[A_1(t)+A_2(t)]$. In Figs. 7(a)–(d) we display the resulting calculated line shapes. The experimental results for Xe/Ne and Xe/He also reproduced in Figs. 7(a)–(d) are in fair agreement (at least at high densities) with the line shape calculated when three-body correlation effects are incorporated.

VI. SOLVENT PERTURBATIONS OF THE DOUBLET SPLITTING OF Xe

In the foregoing discussion we have treated solvent perturbations of the Xe($^3P_1$) and Xe($^1P_1$)[8] impurity states perturbed by rare-gas fluids by assigning a distinct pair-interaction potential to each of the two components of the Xe doublet. The density dependence of the Xe doublet splitting in fluid Ne and Ar is portrayed in Figs. 8 and 9. In these figures we have displayed both the difference between the band maxima and the first moments now calculated from the experimental data on an absolute energy scale, together with the theoretical values for the difference in the first moments calculated from Eq. (II.14a) together with the potential parameters of Table II. The reasonable agreement between the experimental and the theoretical doublet splitting does not provide us with any new information as the excited state potentials were derived by fitting the shifts (and dispersion) for each of the two components of the Xe doublet. What is interesting is the gradual decrease of the doublet splitting, ΔE, relative to the atomic value $\Delta E_0=1.13$ eV[27] with increasing density of Ne and of Ar. At the highest densities attained by us we have $\Delta E/\Delta E_0=0.95$ in Ne at $\rho=0.65$ g cm^{-3} and $\Delta E/\Delta E_0=0.85$ in Ar at $\rho=1.4$ g cm^{-3}. This observation is of interest in relation to the assignment of the two members of the Xe doublet in liquid in in solid rare-gases. In this context it is worth while to point out that a recent comprehensive study of Xe impurity

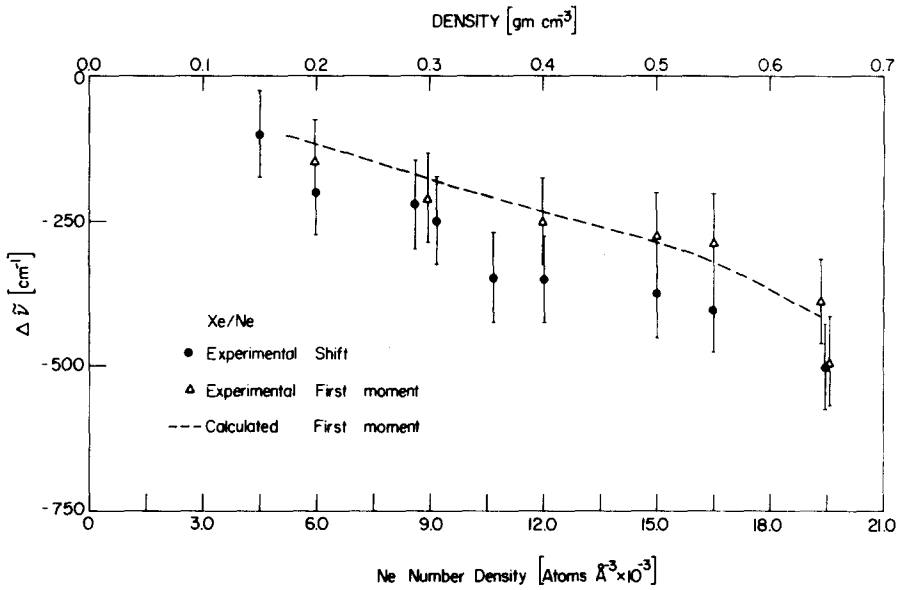

FIG. 8. Density dependence of the change in the Xe doublet splitting $\Delta\tilde{\nu} = \Delta E - \Delta E_0$ in Ne. Points represent experimental data and the dashed curve is the calculated result using "best fit" potential (Table II).

states in solid Ne conducted by Pudewill *et al.*[24] resulted in a reassignment of the $Xe(^1P_1)$ level originally observed by Baldini.[25] Pudewill and colleagues[24] have concluded that in this system $\Delta E - \Delta E_0 = -1300\ \text{cm}^{-1}$ (and $\Delta E/\Delta E_0 = 0.86$), a result which is compatible with a rough linear extrapolation of our data (Fig. 8) for the Xe/Ne system at lower densities up to the solid ($\rho = 1.44\ \text{g cm}^{-3}$) density.

In the case of Xe the major contribution to ΔE originates from spin–orbit coupling λ and thus in many qualitative discussions it was asserted that $\Delta E \cong \lambda$. Theoretical studies of medium effects on the spin–orbit coupling in solids[26] resulted in the conclusion that nonorthogonality corrections result in a modest increase of λ relative to the gas phase value $\lambda_0 = 1.18$ eV,[27,28] so that $\lambda_0 \leq \lambda \leq 1.01\lambda_0$. More elaborate studies by Knox and Inchauspé[29] and by Onodera and Toyozawa[30] of the halogen doublet of alkali halides within the framework of the intermediate coupling scheme, a problem equivalent to the Xe doublet, resulted in $\Delta E_m = 2\sqrt{2}\,\lambda/3$ for the minimum doublet splitting.[30] On the basis of these theoretical studies[26,29,30] we expect that the experimental Xe doublet splitting in a dense medium will satisfy the condition $\Delta E/\Delta E_0 > \alpha_m \equiv 2\sqrt{2}\,\lambda_0/3\Delta E_0 = 0.98$. This prediction is not borne out by our experimental results for Xe in Ar and in Ne fluids and for the Xe impurity state in solid Ne[24] where in all cases the experimental value of $\Delta E/\Delta E_0$ is lower than α_m. A way out of this difficulty is to incorporate medium-induced shifts which are different for the two spin–orbit split components of the Xe atom in a dense medium. This is just the procedure adopted in Sec. IV. Several questions arise at this state. First, and most important, we would like to raise the issue whether our treatment of solvent perturbations of the Xe doublet, which rests on the notion of independently perturbed two-excited level system, is self-consistent. As it is well known these two states corresponding to the allowed transitions of the Xe doublet should be treated via the inter-

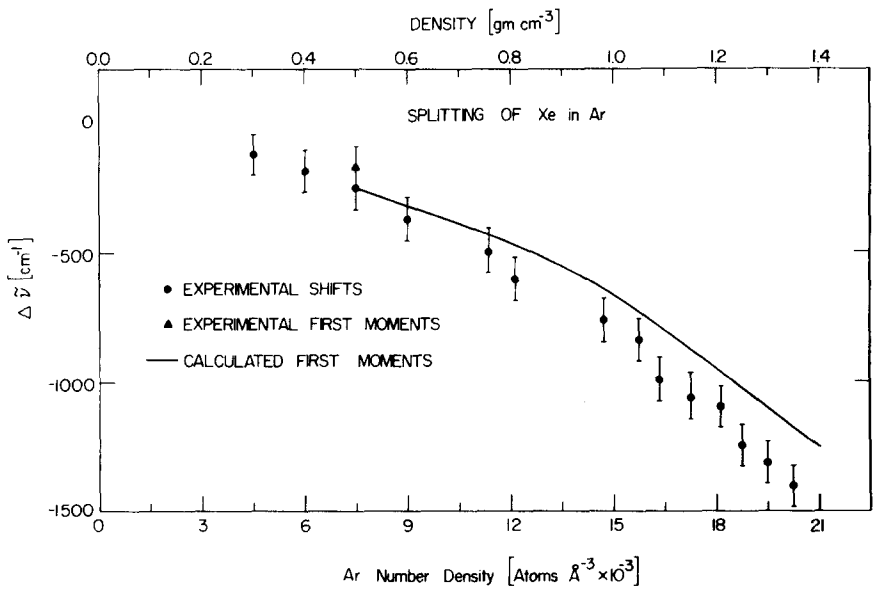

FIG. 9. Density dependence of the change in the Xe doublet splitting $\Delta\tilde{\nu} = \Delta E - \Delta E_0$ in Ar. Points represent experimental data and the dashed curve is the calculated result using "best fit" potential (Table II).

mediate coupling scheme, and it is an open question whether solvent perturbation can be handled independently. Second, can one provide a self-consistent interpretation of both the splitting and the intensity ratio of the Xe doublet perturbed by Ar and Ne. We shall now address ourselves to these problems.

VII. INTERMEDIATE COUPLING SCHEME FOR SOLVENT PERTURBATIONS OF THE Xe DOUBLET

It is well known that the doublet splitting and the intensity ratio of the two doublet components of atomic Xe can be described in terms of the intermediate coupling scheme[26,29,30] and a similar approach should be readily adopted to Xe impurity in the condensed phase. We start from the (J_c, j) coupling scheme, appropriate for a heavy atom like Xe (where J_c is the total angular momentum of the ionic core and j corresponds to the angular momentum of the excited electron). The appropriate zero order lowest excited states of Xe correspond to $|1\rangle = (\frac{1}{2}, \frac{1}{2})$, and $|2\rangle = (\frac{3}{2}, \frac{1}{2})$, which in the isolated atom are split by the spin–orbit coupling λ_0, while the electron-hole exchange interaction Z_0 mixes the (zero order) states $|1\rangle$ and $|2\rangle$. When the Xe atom is perturbed by an external medium the spin–orbit coupling λ and the electron–hole exchange interaction Z are expected to be density dependent. Theoretical calculations on Ar impurity states in solid rare-gases[26] indicate that λ in the solid is about the same as λ_0, so that density dependence of λ is weak. No complementary information is available regarding the density dependence of Z. When medium induced perturbation of the Xe doublet are described just by the density-dependent energetic parameters Z and λ, the minimum splitting rule $\Delta E_m = 2\sqrt{2}\lambda/3$ is violated in the Xe/Ar and in the Xe/Ne systems, as discussed in Sec. VI. We have provided a straightforward extension of the intermediate coupling scheme for medium-perturbed Xe by incorporating two (diagonal) density dependent energy shifts, ϵ_1 and ϵ_2 of the (zero order) states $|1\rangle$ and $|2\rangle$, respectively. We note in passing that ϵ_1 and ϵ_2 which specify the perturbation of the zero order states, not included in Z are distinct from the experimental and theoretical values of $\Delta(^3P_1)$ and $\Delta(^1P_1)$. The interaction matrix in the (J_c, j) representation is[30]

$$\begin{matrix} & (\frac{1}{2},\frac{1}{2}) & (\frac{3}{2},\frac{1}{2}) \\ (\frac{1}{2},\frac{1}{2}) & 2\lambda/3 + Z/3 + \epsilon_1 & \sqrt{2}Z/3 \\ (\frac{3}{2},\frac{1}{2}) & \sqrt{2}Z/3 & -\lambda/3 + 2Z/3 + \epsilon_2 \end{matrix} \qquad \text{(VII. 1)}$$

The resulting experimental energy levels of the states $|A\rangle$ and $|B\rangle$ of the system expressed in increasing orders are

$$E_A = \tfrac{1}{2}\{Z + \lambda/3 + \epsilon_1 + \epsilon_2 - U(1+4W^2)^{1/2}\}, \qquad \text{(VII. 2)}$$
$$E_B = \tfrac{1}{2}\{Z + \lambda/3 + \epsilon_1 + \epsilon_2 + U(1+4W^2)^{1/2}\},$$

while the splitting $\Delta E = E_B - E_A$ and the intensity ratio I_A/I_B are

$$\Delta E = U(1+4W^2)^{1/2}, \qquad \text{(VII. 3)}$$

$$I_A/I_B = \left[\frac{2\sqrt{2}(1+4W^2)^{1/2} - 6W}{3 - (1+4W^2)^{1/2}}\right]^2, \qquad \text{(VII. 4)}$$

where

$$U = \lambda + \epsilon_1 - \epsilon_2 - Z/3, \qquad W = \frac{\sqrt{2}Z}{3(\lambda + \epsilon_1 - \epsilon_2) - Z}. \qquad \text{(VII. 5)}$$

From Eqs. (VII. 2)–(VII. 4) it is evident that, in general, when the $|1\rangle$ and the $|2\rangle$ states are strongly scrambled one cannot assign spectral shifts in terms of additive contribution to the energy levels $|A\rangle$ and $|B\rangle$ of the isolated Xe atom. Such a procedure is justified only for limiting situations. In the present case we assume that $a = Z/\lambda \ll 1$ and $b = |\epsilon_1 - \epsilon_2|/\lambda \ll 1$. The first inequality originates from the data for atomic Xe[27] where $Z_0/\lambda_0 = 0.22$ while the second condition is justified on the basis of the data of Figs. 8 and 9 as $|\epsilon_1 - \epsilon_2| \sim |\Delta E - \Delta E_0| \leq 1000\ \text{cm}^{-1}$ so that $b \sim |\Delta E - \Delta E_0|/\lambda_0 \simeq 0.1$. Expansion of Eqs. (VII. 2)–(VII. 4) to second order in $1/\lambda$ results in

$$E_A = -\lambda/3 + \epsilon_2 + 2Z/3 - \frac{2}{g}\frac{Z^2}{\lambda}\left(1 - \frac{\epsilon_1 - \epsilon_2}{\lambda}\right) \qquad \text{(VII. 6a)}$$
$$E_B = 2\lambda/3 + \epsilon_1 + Z/3 + \frac{2}{g}\frac{Z^2}{\lambda}\left(1 - \frac{\epsilon_1 - \epsilon_2}{\lambda}\right)$$

$$\Delta E = U\left[1 + \frac{4}{g}(Z/\lambda)^2 + \cdots\right] \qquad \text{(VII. 6b)}$$

$$I_A/I_B = 2 - 4(Z/\lambda) + \frac{4Z(\epsilon_1 - \epsilon_2)}{\lambda^2} + \frac{14}{3}\left(\frac{Z}{\lambda}\right)^2. \qquad \text{(VII. 6c)}$$

Taking as rough estimates $a = 0.25$, $Z \sim 0.25$ eV as appropriate for atomic Xe and $b \sim 0.1$ the last term on the rhs of Eq. (VII. 6a) can be neglected, thus the spectral shifts are

$$\Delta(^1P_1) = E_B - \hbar\omega_0 = \epsilon_1 + \tfrac{2}{3}(\lambda - \lambda_0) + \tfrac{1}{3}(Z - Z_0),$$
$$\Delta(^3P_1) = E_A - \hbar\omega_0 = \epsilon_2 - \tfrac{1}{3}(\lambda - \lambda_0) + \tfrac{2}{3}(Z - Z_0). \qquad \text{(VII. 7)}$$

The density dependence of ϵ_1, ϵ_2, λ, and Z, all of which appear as linear terms in Eq. (VII. 7) is incorporated in the effective pair potentials advanced in Secs. II and IV. The weak density dependence of λ can be probably neglected (setting $\lambda = \lambda_0$) and the major contributions to the guest–host interaction potentials originate from electrostatic and exchange terms. These considerations provide a justification for the application of the

TABLE III. Density dependence of the integrated intensity ratio $(^3P_1/^1P_1)$ of the Xe doublet perturbed by Ne.

Temp. (°K)	Ne Density (g cm^{-3})	Intensity Ratio[b]
295	0.1	1
165	0.16	1.6
105	0.22	1.5
225	0.28	1.6
175	0.32	1.3
140	0.37	1.6
150	0.41	1.75
110	0.44	1.5
88	0.51	1.5
78	0.55	1.7
70	0.65	1.8
6	1.44 (solid)	1.9[a]

[a]Reference 25.
[b]Accuracy of intensity ratios for perturbed Xe, ±0.2.

statistical theory to the components of the Xe doublet.

To obtain some idea regarding the density dependence of Z we finally consider the intensity ratio I_A/I_B [i.e., to the $^3P_1$ and to $^1P_1$ states in the notation of Section (I.–IV.)]. In Table III we present our experimental results for the Xe/Ne system, where reasonably accurate data (within ± 15%) would be obtained by numerical integration of the spectra of Fig. 4. The intensity ratio increases from $I_A/I_B = 1.0$ at $\rho = 0$ [31] to $I_A/I_B = 1.5 \pm 0.2$ at $\rho = 0.15$ g cm^{-3} exhibiting a further slow increase with increasing ρ up to the value $I_A/I_B = 1.8 \pm 0.2$ at $\rho = 0.65$ g cm^{-1}, while in solid Ne[25] $I_A/I_B \cong 1.9$. For Xe it is sufficient to take Eq. (VII.6c) in the form $I_A/I_B \simeq 2 - 4(Z/\lambda)$, and the dependence of the intensity ratio on $|\epsilon_1 - \epsilon_2|/\lambda$ is negligible. For atomic Xe we thus have $Z_0/\lambda_0 \simeq 0.22$ and $I_A/I_B \cong 1.0$. The increase of I_A/I_B from the value of 1.0 to 1.8 ± 0.2 over the Ne density range 0–0.65 g cm^{-3} implies that Z/λ decreases from 0.22 to 0.05 ± 0.05 over this density range. Medium perturbations result in a decrease of Z from $Z_0 \simeq 0.25$ eV at $\rho = 0$ to $Z \simeq 0.04 \pm 0.04$ eV in the dense fluid at $\rho = 0.65$ g cm^{-3}, and a similar small value of Z is also appropriate for the solid. This density dependence of the electron–hole exchange together with the incorporation of the density dependent diagonal energy shift ϵ_1 and ϵ_2 provide a semiquantitative self-consistent interpretation of the splitting and of the intensity ratio of the medium perturbed Xe doublet.

[1] (a) H. Margenau, Phys. Rev. **48**, 755 (1935); (b) H. Margenau, Phys. Rev. **82**, 156 (1951); (c) H. Margenau and H. C. Jacobson, J. Quant. Spectrosc. Radiat. Transfer **3**, 35 (1963); (d) F. Schuller and W. Behmenburg, Physics Reports, Phys. Lett. Sect. C **12**, 273 (1974).

[2] J. Robin, R. Bergeon, L. Galatry, and B. Vodar, Discuss. Faraday Soc. **22**, 30 (1956).

[3] G. D. Mahan, Phys. Rev. A **6**, 1273 (1972).

[4] M. J. Saxton and J. M. Deutch, J. Chem. Phys. **60**, 2800 (1974).

[5] I. Messing, B. Raz, and J. Jortner, in *Vacuum Ultraviolet Radiation Physics*, edited by E. E. Koch, R. Haensel, and C. Kunz, (Pergamon–Viewveg, 1974), p. 40.

[6] I. Messing, B. Raz, and J. Jortner, "Medium Perturbations of Atomic Extravalence Excitations," J. Chem. Phys. (in press).

[7] O. Cheshnovsky, B. Raz, and J. Jortner, J. Chem. Phys. **59**, 5471 (1973).

[8] Xe[$^3P_1$) and Xe[$^1P_1$] designate the $6s[^3/_2]$ $J=1$ and $6s'[\frac{1}{2}]$ $J=1$ states of the atomic Xe configurations $5p^5[^2P_{3/2}]6s$ and $5p^5[^2P_{1/2}]6s$, respectively, according to C. E. Moore, US Natl. Bur. Stand., Circ. **467** (1958).

[9] R. Kubo and Y. Toyozawa, Prog. Theoret. Phys. (Jpn) **13**, 160 (1955).

[10] M. Born and A. S. Green, Proc. R. Soc. (London) Ser. A **188**, 10 (1946).

[11] R. P. Futrelle, Phys. Rev. A **5**, 2162 (1972).

[12] N. H. March, "The Liquid State" in *Theory of Condensed Matter* (International Center for Theoretical Physics, Trieste, 1967).

[13] M. Lax, J. Chem. Phys. **20**, 1752 (1952).

[14] (a) R. E. Huffman, S. L. Larrabee, and Y. Tanaka, Appl. Opt. **4**, 1581 (1965); (b) B. Raz, J. Magen, and J. Jortner, Vacuum **19**, 571 (1969).

[15] *Argon, Helium and the Rare Gases*, edited by G. A. Cook (Interscience, New York, 1961), Vol. I., p. 261–263.

[16] R. D. McCarty and R. B. Stewart, in *Advances in Thermophysical Properties at Extreme Temperatures and Pressures*, Purdue University, West Lafayette, 1965), p. 84–97.

[17] (a) M. C. Castex, R. Granier, and J. Romand, CR Acad. Sci. (Paris) Ser. B **268**, 552 (1969); (b) M. Morlais, J. M. Rupin, A. Quemerais, S. Robin, CR Acad. Sci. (Paris) Ser. B **269**, 1223 (1969); (c) I. Messing, M. Sc. thesis, Tel-Aviv University, Israel, 1970.

[18] I. Messing, B. Raz, and J. Jortner, "Experimental evidence for Wannier Impurity States in Doped Rare-gas Fluids" (to be published).

[19] (a) W. Hogervorst, Physica **51**, 90 (1971); (b) B. Schneider, J. Chem. Phys. **58**, 4447 (1973).

[20] G. J. Throop and R. J. Bearman, J. Chem. Phys. **42**, 2408 (1965).

[21] G. J. Throop and R. J. Bearman, J. Chem. Phys. **42**, 2838 (1965).

[22] F. Mandel, R. J. Bearman, and M. Y. Bearman, J. Chem. Phys. **52**, 3315 (1970).

[23] (a) A. Royer, Phys. Rev. A **4**, 499 (1971); (b) J. Szudy and W. E. Baylis, J. Quant. Spectrosc. Radiat. Transfer **15**, 641 (1975).

[24] D. Pudewill, F. J. Himpsel, V. Saile, N. Schwentner, M. Skibowsky, and E. E. Koch, Phys. Status Solidi B **74**, 485 (1976).

[25] G. Baldini, Phys. Rev. **137**, 508 (1965).

[26] (a) R. S. Knox, J. Phys. Chem. Solids **9**, 265 (1959); (b) A. Gold, *ibid.* **18**, 218 (1961).

[27] R. S. Knox, Phys. Rev. **110**, 375 (1958).

[28] We utilize here the spin–orbit coupling matrix element in the form introduced in Ref. 30. In the usual atomic formulation (Ref. 27) two spin–orbit interaction parameters appear: The spin–orbit coupling ζ and the King Van-Vleck parameter which is 1.055 for Xe (Ref. 27). Therefore, $\lambda = 1.56\ \zeta$.

[29] R. S. Knox and N. Inchauspé, Phys. Rev. **116**, 1093 (1959).

[30] Y. Onodera and Y. Toyozawa, J. Phys. Soc. (Jpn) **22**, 833 (1967).

[31] P. G. Wilkinson, J. Quant. Spectrosc. Radiat. Transfer **6**, 823 (1966).